Available online at www.sciencedirect.com

SciVerse ScienceDirect

Geochimica et Cosmochimica Acta 103 (2013) 11–25

Geochimica et Cosmochimica Acta

www.elsevier.com/locate/gca

Evolution of carbon cycle over the past 100 million years

Gaojun Li [a,*], Henry Elderfield [b]

[a] MOE Key Laboratory of Surficial Geochemistry, Department of Earth Sciences, Nanjing University, Nanjing 210093, China
[b] The Godwin Laboratory for Palaeoclimate Research, Department of Earth Sciences, University of Cambridge, Downing Street, Cambridge CB2 3EQ, UK

Received 24 November 2011; accepted in revised form 9 October 2012; available online 17 October 2012

Abstract

It is generally accepted that progressive cooling of global climate since the Late Cretaceous results from decreasing partial pressure of atmospheric CO_2 (pCO_2). However, details on how and why the carbon cycle evolved and how it would affect pCO_2 have not been fully resolved. While the long-term decline of pCO_2 might be caused by the decrease of volcanic degassing through the negative feedback between pCO_2 and silicate weathering, seafloor spreading, the major control of CO_2 degassing, seems to have remained relatively constant. Alternative explanation, known as 'uplift driven climate change' hypothesis, proposes that tectonic uplift may have enhanced the sink of atmospheric CO_2 by silicate weathering, and thus produced the decline of pCO_2. However, increasing weathering sink of CO_2 could deplete atmosphere all of its CO_2 within several million years while holding volcanic outgassing constant. In this work, major fluxes of long-term carbon cycle are calculated based on a reverse model constrained by marine C, Sr and Os isotopic records and the spreading rate of sea floor. Weathering of island basalt and continental silicate rocks are separated in the new model. The results indicate a long-term decline of island basalt weathering in consistent with the global cooling trend over the past 100 million years. Dramatic changes of the CO_2 fluxes associated continental silicate weathering, reverse weathering, volcanic degassing and the growth of organic carbon reservoir have been observed. Disturbance of atmospheric CO_2 cycle by these fluxes seems to be maintained by the concomitant adjustments of island basalt weathering that were sensitive to the pCO_2 controlled environment factors such as temperature and runoff. The negative feedbacks between pCO_2 and weathering of island basalt might have played a significant role in stabilizing the long-term carbon cycle.

1. INTRODUCTION

Global climate has experienced dramatic change since the Late Cretaceous. During the latest portion of Cretaceous approximately 100–65 million years ago, global temperature reached the highest level of the last ~200 million years with no glaciation in both poles (Bice et al., 2006). Progressive cooling afterward transited the earth from a greenhouse state into an icehouse world with ice caps at high latitudes, first in Antarctic and later in the North Hemisphere (Zachos et al., 2001). It is believed that decreasing partial pressure of CO_2 in atmosphere (pCO_2) is the primary determinant for the long-term cooling trend and for the growth of continental-scale ice sheet in polar regions (Deconto and Pollard, 2003). Although growing evidences confirmed a long-term decrease of pCO_2 (Pearson and Palmer, 2000; Pagani et al., 2005; Tripati et al., 2009), the reason behind the decline of pCO_2 is still under debates.

Reduction of CO_2 degassing has been proposed by BLAG carbon cycle model as the primary driver for the decline of pCO_2 through the negative feedbacks between pCO_2 and silicate weathering (Berner et al., 1983). In this model, weathering reaction is largely controlled by the climatic factors that are sensitive to the changes of pCO_2, such as temperature and runoff. Thus, balance of carbon cycle could be maintained by the negative feedbacks between

* Corresponding author.
E-mail address: ligaojun@nju.edu.cn (G. Li).

0016-7037/$ - see front matter © 2012 Elsevier Ltd. All rights reserved.
http://dx.doi.org/10.1016/j.gca.2012.10.014

pCO_2 and silicate weathering (Walker et al., 1981; Berner et al., 1983). Due to the limited capacity of atmosphere, a decrease of CO_2 outgassing would result in rapid drop of pCO_2 until new balance is reached so that the decreasing CO_2 consumption by silicate weathering in response to the decline of pCO_2 could compensate the reduction of CO_2 degassing. However, the rate of sea floor spreading, which is believed as the major control of CO_2 degassing (Berner et al., 1983), have remained relatively constant especially over the past 65 million years (Rowley, 2002; Muller et al., 2008).

Alternative explanation, known as 'uplift driven climate change' hypothesis (Raymo et al., 1988; Raymo and Ruddiman, 1992), suggested that the late Cenozoic tectonic uplift, mainly Tibetan Plateau, may have enhanced physical erosion and monsoonal rainfall, which finally helped drawdown of atmospheric CO_2 by silicate weathering. The post-Eocene decline of pCO_2 and global cooling is coincident with the time of major Cenozoic orogenesis (Raymo and Ruddiman, 1992). Increasing production of terrigenous sediment and raising $^{87}Sr/^{86}Sr$ and $^{187}Os/^{188}Os$ ratios of seawater also support a late Cenozoic increase in both physical and chemical denudation (Hay et al., 1988; Edmond, 1992; Peucker-Ehrenbrink et al., 1995). However, increasing weathering sink of CO_2 would deplete atmosphere all of its CO_2 within several million years while holding volcanic outgassing constant (Berner and Caldeira, 1997).

The 'uplift driven climate change' hypothesis argues that the sequestration of atmosphere CO_2 by silicate weathering is a strong function of continental relief, and the importance of pCO_2-weathering feedback which prevents runaway icehouse or greenhouse in BLAG carbon cycle model is implicitly negated (Raymo and Ruddiman, 1992). As no evidence pointing an increase of volcanic degassing, two potential negative feedbacks were proposed to compensate the increasing erosional drawdown of CO_2 (Raymo and Ruddiman, 1992): (1) decreasing accumulation of sedimentary organic carbon due to increasing oxygen concentration of seawater in response to climate cooling (Raymo, 1994); (2) increasing precipitation of silicate minerals in the deep sea or decreasing weathering of seafloor basalt in response to the elevated pH of seawater under lower pCO_2 (Francois and Walker, 1992). However, growth of organic carbon reservoir seems to have increased as a result of increasing preservation efficiency in regions with high sedimentation rate of terrigenous materials (France-Lanord and Derry, 1997). Precipitation of silicate minerals in the deep sea, known as reverse weathering, may be largely controlled by the supply of degraded weathering product (Michalopoulos and Aller, 1995). Although reverse weathering may increase in response to increasing weathering product, it cannot compensate all of the increasing consumption of CO_2 by continental silicate weathering since the net effect of weathering and reverse weathering should remove CO_2 from atmosphere. The dynamics of seafloor basalt weathering is poorly understood and is supposed to be largely controlled by the spreading rate of seafloor rather than pH (Wallmann, 2001).

The fundamental difference between BLAG carbon model (Berner et al., 1983) and the 'uplift driven climate change' hypothesis (Raymo and Ruddiman, 1992) is related to the two extreme mechanisms that control the rate of silicate weathering, i.e., the weathering limited regime and the supply limited regime respectively. Weathering regime largely depends on the extent of physical erosion (Kump et al., 2000; West et al., 2005). Under the weathering limited regime, fresh rocks are sufficiently exposed and weathering rate is controlled by kinetic parameters of weathering reaction that are closely linked to pCO_2, e.g., temperature. While under the supply limited weathering regime, physical erosion is weak, weathering of fresh rock is inhibited by the protection of soil cover and weathering rate largely depends on the rate of physical erosion (Kump et al., 2000; West et al., 2005).

Generally, the large continents are not effectively eroded, weathering of continental silicate seems to be largely supply limited (Gaillardet et al., 1999). Kump and Arthur (1997) argued that the increasing sequestration of atmospheric CO_2 in active orogens such as Himalayas may has been offset by reduction of weathering elsewhere under a kinetically controlled weathering regime due to the decline of temperature and runoff in response to the drop of pCO_2. Weathering of island basalt may play a significant role in this mechanism. Most of the oceanic islands locate at tectonically active regions, and are generally characterized by mountainous relief with particularly high rate of physical erosion (Milliman and Meade, 1993). Thus, weathering of island basalt might be largely subjected to the weathering limited regime, which shows high weathering flux and strong environmental influence such as temperature, runoff and plant cover (Moulton and Berner, 1998; Dessert et al., 2003; Louvat et al., 2008; Gaillardet et al., 2011; Schopka et al., 2011). Updated estimates on the cumulative surface area and weathering rate of island basalt (Dessert et al., 2003; Allègre et al., 2010) indicate that weathering of island basalt consumes up to 5.0×10^{12} mol atmospheric CO_2 per year at the present, which is more than half of that consumed by continental silicate weathering (Gaillardet et al., 1999). This value might be even higher when the underground weathering flux is considered (Schopka and Derry, 2012). Thus, weathering of island basalt may act an important role in regulating the long-term balance of carbon cycle through the pCO_2-weathering feedbacks.

Marine isotopic records of carbon, strontium and osmium could help resolve the ancient carbon cycle processes because carbon fluxes derived from different reservoirs are characterized by distinct $\delta^{13}C$ values and the processes that control the long-term carbon cycle also control the strontium and osmium isotopic compositions of seawater. A set of early works has established the framework to calculate ancient carbon cycle fluxes mainly based on marine C and Sr isotopic records (Kump, 1989; Derry and France-Lanord, 1996; Goddéris and François, 1996; Kump and Arthur, 1997; Francois and Goddéris, 1998; Wallmann, 2001; Berner, 2006; Kashiwagi et al., 2008). In these works, normally four equations were involved regarding the mass balances of carbon and alkalinity, and the isotopic balances of carbon and strontium in ocean–atmosphere system. Some works may favor the mass balance equation of atmospheric CO_2 instead of oceanic alkalinity. As a matter of fact, mass balance equation of atmospheric CO_2 could be

deduced by combining the mass balance equations of alkalinity and total carbon in ocean–atmosphere system. Theoretically, only four fluxes of carbon cycle could be computed independently from the four mass balance equations. Simplifications have to be made to reconstruct the entire carbon cycle. For example, volcanic degassing of CO_2 is normally constrained by the spreading rate of mid-ocean ridges or hold as constant. Li et al. (2009) implemented osmium isotopic balance as an additional constrain. By doing so, they were able to calculate volcanic degassing. However, the reconstructed CO_2 degassing show dramatic decrease during the early Cenozoic (Li et al., 2009), which is quite unrealistic considering the nearly constant spreading rate of sea floor (Rowley, 2002).

This work readopts the traditional way to constrain the hydrothermal fluxes and CO_2 degassing by the spreading rate of sea floor. The rest of the freedom in the model of Li et al. (2009) is then used to separate the weathering of island basalt from total silicate weathering. Neutralization of oceanic alkalinity by the acidity released by hydrothermal fluids and/or reverse weathering is also considered. Mg cycle is incorporated to reproduce the concentration of seawater Mg as a secondary driver for hydrothermal flux and as an extra testing target for the model results. The ultimate goal of this work is to resolve the factors that drove the secular changes of global carbon cycle over the past 100 million years, to find out the mechanism that maintained a long-term balance of atmospheric CO_2 budget, and to answer how the changes of carbon cycle would control the concentration of atmospheric CO_2 and thus global temperature.

2. METHOD

2.1. Mass balance equations

The long-term carbon cycle in this model mainly involve eight processes, namely (1) continental silicate weathering, (2) carbonate weathering, (3) weathering of organic carbon in sedimentary rocks, (4) weathering of island basalt, (5) carbonate sedimentation, (6) burial of sedimentary organic carbon, (7) H^+ released by hydrothermal alternation and/or reverse weathering, and (8) volcanic degassing of CO_2. These processes often have opposite effects on carbon cycle. Carbonate weathering provides carbon and bicarbonate alkalinity to the ocean, which is then removed by burial of carbonate in sediment or oceanic crust. The two processes could be expressed as a reversible reaction:

$$Ca(Mg)CO_3 + CO_2 + H_2O \Longleftrightarrow Ca^{2+}(Mg^{2+}) + 2HCO_3^- \quad (1)$$

Silicate weathering and the acidity (H^+) released by hydrothermal alternation or reverse weathering also act in an opposite way. Production of H^+ by hydrothermal alternation and/or reverse weathering can be simplified as the formation of brucite layer in serpentine or authigenic clay minerals:

$$Mg^{2+} + 2H_2O \rightarrow Mg(OH)_2 + 2H^+ \quad (2)$$

Atmospheric CO_2 is fixed into bicarbonate by silicate weathering while the H^+ released by hydrothermal alternation and/or reverse weathering converts bicarbonate back to atmosphere:

$$Silicate + CO_2 + H_2O \rightarrow Cations + HCO_3^- + Degraded\ products \quad (3)$$

$$HCO_3^- + H^+ \rightarrow H_2O + CO_2 \quad (4)$$

Also, oxidation and burial of sedimentary organic carbon can be simplified as reversal processes of respiration and photosynthesis:

$$CH_2O + O_2 \Longleftrightarrow CO_2 + H_2O \quad (5)$$

Carbon in the ocean–atmosphere system has a residence time of about $\sim 10^4$ years (Berner and Caldeira, 1997). On time scale of million years, the ocean–atmosphere system could be treated as steady state with respect to carbon. All of the carbon inputted into the system should be equally removed. Volcanic degassing, carbonate weathering and oxidation of organic sediments are the primary sources of carbon, which are mainly removed by burial of organic matter and carbonate in sediment or oceanic crust. The mass balance and isotopic balance of total carbon in the ocean–atmosphere system can thus be expressed as:

$$\sum(K_i \times C_i) = \sum(K_j \times C_j) \quad (6)$$

$$\sum(K_i \times C_i \times \delta^{13}C_i) = \sum(K_j \times C_j \times \delta^{13}C_j) \quad (7)$$

where K is relative intensity to Late Pleistocene values for the processes labeled by corresponding subscripts (same for rest of the work); C is Late Pleistocene carbon fluxes associated with these processes; $\delta^{13}C$ is corresponding carbon isotopic composition. Subscripts i include *carbw* (carbonate weathering), *orgw* (weathering of organic carbon), *ma* (CO_2 degassing from mid-ocean ridge and arc volcanoes), and *plume* (plume CO_2 degassing). The total volcanic degassing of CO_2 (*ma* + *plume*) is labeled by *volc* in Tables 2 and 3. Subscripts j include *carbb* (carbonate burial), and *orgb* (burial of organic carbon).

Bicarbonate alkalinity in the ocean also has a very short residence time similar to that of total carbon. Likewise, alkalinity provided by rock weathering should be sunk by carbonate sedimentation and neutralization of H^+ on time scale of million years:

$$\sum(K_i \times A_i) = \sum(K_j \times A_j) \quad (8)$$

where A is Late Pleistocene fluxes of alkalinity associated with the processes labeled by corresponding subscripts. Subscripts i include *csiliw* (continental silicate weathering), *basw* (weathering of island basalt), and *carbw* (carbonate weathering). Subscripts j includes *carbb* (carbonate burial), and *rev* (alkalinity neutralization by the H^+ released from hydrothermal alternation and reverse weathering, which are termed as reverse weathering for simplification).

Main inputs of strontium to the oceans are related to rock weathering, hydrothermal activity, and diagenetic products of marine sediments. A transient-state solution to the strontium isotopic composition of seawater is shown below (Hodell et al., 1989):

$$N \times dR^{Sr}_{ocean}/dt = \sum \left[K_i \times Sr_i \times (R^S_i - R^{Sr}_{ocean})\right] \quad (9)$$

where R^{Sr} is normalized strontium isotopic composition (atomic fraction of ^{87}Sr) that enables accurate mass balance calculation: $R^{Sr} = (^{87}Sr/^{86}Sr)/(9.43 + ^{87}Sr/^{86}Sr)$; N is the amount of strontium in seawater; dR^{Sr}_{ocean}/dt describes the changing rate of R^{Sr} of seawater; Sr is the Late Pleistocene Sr fluxes associated with the processes labeled by corresponding subscripts, which include *csiliw* (continental silicate weathering), *basw* (weathering of island basalt), *carbw* (carbonate weathering), *hy* (hydrothermal activity), and *dia* (sediment diagenesis).

Osmium in oceans is sourced from rock weathering, hydrothermal input, and cosmic flux to a lesser extent. Due to short residence time of about several 10^4 years (Levasseur et al., 1999), osmium in seawater would reach a steady state on time scale of million years and the time derivative in the oceanic osmium isotopic budget could be neglected. Thus, the osmium isotopic composition of seawater can be calculated by averaging the osmium isotopic composition of all osmium inputs to the oceans in a weighted manner:

$$\sum \left[K_i \times Os_i \times (R^{Os}_i - R^{Os}_{ocean})\right] = 0 \quad (10)$$

where R^{Os} is normalized osmium isotopic composition (atomic fraction of ^{187}Os) that enable accurate mass balance calculation: $R^{Os} = (^{187}Os/^{188}Os)/(7.4 + ^{187}Os/^{188}Os)$; R^{Os}_{ocean} is Os isotopic composition of seawater; Os is Late Pleistocene Os fluxes associated with the processes labeled by corresponding subscripts, which include *csiliw* (continental silicate weathering), *basw* (weathering of island basalt), *sediw* (weathering of sedimentary rocks), *hy* (hydrothermal activity), *cos* (cosmic input).

Considering that Mg is the major reactant in hydrothermal reaction and reverse weathering (Michalopoulos and Aller, 1995; Elderfield and Schultz, 1996), the activities of hydrothermal reaction (K_{hy}) and reverse weathering (K_{rev}) may be largely controlled by seawater Mg concentration in addition to the spreading rate of mid-ocean ridges (Sp):

$$K_{hy} = K_{rev} = CMg_t/CMg_0 \times Sp \quad (11)$$

where CMg_t and CMg_0 are Mg concentration of seawater of the past and today respectively. Concentration of Mg in seawater is modeled by assuming that the removal of Mg by hydrothermal alternation and reverse weathering is proportional to Mg concentration of seawater and spreading rate of sea floor:

$$V \times \mathrm{dCMg_t/dt} = \sum(K_i \times \mathrm{Mg_i}) - \mathrm{CMg_t/CMg_0} \times \mathrm{Sp} \times \mathrm{Mg_{hy}} \quad (12)$$

where V is the volume of ocean; Mg with corresponding subscripts showing the Late Pleistocene Mg flux associated with rock weathering and removal of hydrothermal alternation (Mg_{hy}). Subscripts i includes *csiliw* (continental silicate weathering), *basw* (weathering of island basalt), *carbw* (carbonate weathering).

2.2. Model simplification

Eqs. (6)–(12) involve more than 10 processes (Table 1). Theoretically, only seven processes could be solved simultaneously from Eqs. (6)–(12) given that other parameters in the equations are known and simplification are made to confine rest of the processes. One reasonable simplification is to combine carbonate weathering (K_{carbw}), weathering of organic carbon (K_{orgw}) and weathering of sedimentary rocks (K_{sediw}) together after Derry and France-Lanord (1996), since on large scale, sedimentary rocks such as limestone and organic-rich layers are interbedded. As many believed (Berner et al., 1983), CO_2 degassing from mid-ocean ridge and arc volcanoes could be constrained by the spreading rate of ocean floor. Plume CO_2 degassing (K_{plume}), diagenetic input (K_{dia}), and cosmic flux (K_{cos}) are kept as constant. A summary of the model simplification could be found in Table 1. As a result of simplification, only six major processes as well as Mg concentration of seawater should be constrained, which satisfies the freedom of Eqs. (6)–(12).

2.3. Data

A comprehensive review is given to define the values of the parameters. Table 2 lists the primary parameters. All of the parameters used in Eqs. (6)–(12) are listed in Table 3, which are either taken from Table 2 directly or calculated from the primary parameters in Table 2. Fig. 1 shows the time dependent parameters, i.e., the marine C, Sr, Os isotopic records and the spreading rate of mid-ocean ridge. Removal of Mg by hydrothermal activity and reverse weathering ($Mg_{hy\&rev}$) in late Pleistocene is tuned to 4.2×10^{12} mol/year so that the modeled Mg concentration of modern ocean could match observation. The best estimate of Mg sink in modern hydrothermal system is about 2.4×10^{12} mol/year (Elderfield and Schultz, 1996). However, large uncertainty may arise from off-axis hydrothermal activities where huge amount of water fluxes through ridge flanks even though the Mg loss is very small under lower temperature (Elderfield and Schultz, 1996). It is interesting to notice that of the 4.2×10^{12} mol/year of Mg removed by hydrothermal system and reverse weathering, only about half is used to released H^+ (4.6×10^{12} mol/year, $A_{hy\&rev}$ in Table 3). Rest of the Mg may be consumed to replace the Ca^{2+} in the oceanic rocks (Wallmann, 2001; Arvidson et al., 2006).

2.4. Error control and sensitive analysis

Traditional methods of error propagation is employed to estimate uncertainties induced by the proposed error of the primary parameters listed in Table 2 (Li et al., 2009):

$$E_i = \mathrm{sqrt}\left[\sum_{n=1,2,\ldots,37} (\partial K_i/\partial P_n \times \sigma_n)^2\right] \quad (13)$$

where E_i is the accumulative error of model result K_i; σ_n is proposed error of the primary parameter P_n in Table 2. The accumulative errors are displayed as shaded envelopes in Fig. 2, which are small compared to the overall trends of the model results.

Sensitivity (η^n_i) of the modeled results on the error of parameters P_n is estimated by integrating the error contribution of σ_n to the square of E_i:

Table 1
Major processes involved in the model and model simplification.

Symbol	Description	Model simplification
K_{csiliw}	Continental silicate weathering	NA
K_{basw}	Island basalt weathering	NA
K_{carbw}	Carbonate weathering	In proportion to each others
K_{orgw}	Weathering of organic carbon	
K_{sediw}	Weathering of sedimentary rocks	
K_{carbb}	Carbonate sedimentation	NA
K_{orgb}	Burial of organic carbon	NA
K_{ma}	Degassing from mid-ocean ridges and arc	In proportion to sea floor spreading rate
K_{rev}	Reverse weathering	In proportion to sea floor spreading rate and seawater Mg concentration
K_{hy}	Hydrothermal fluxes	
K_{plume}	Plume volcanic degassing	Kept as constant
K_{dia}	Diagenetic input	
K_{cos}	Cosmic input	

$$\eta_i^n = \int_0^t (\partial K_i/\partial P_n \times \sigma_n/E_i)^2 \mathrm{dt/t} \quad (14)$$

The results show that error of the model is largely contributed by the uncertainties of spreading rate of sea floor (Fig. 3). Sediment weathering and burial of carbonate and organic carbon are also very sensitive the parameters related to Os cycle (Fig. 3).

Himalayan rivers are characterized by extremely radiogenic strontium isotopic compositions either from silicate or carbonate weathering (Galy et al., 1999; Jacobson and Blum, 2000). Recent compilations of eleven major upper streams leading out Tibetan Plateau yield strontium flux of about 3.2×10^9 mol/year with $^{87}Sr/^{86}Sr$ ratios of about 0.71448 (Wu et al., 2009). Uplift of Tibetan Plateau since about 40 Ma may increase the inputs of Tibetan rivers and thus influence the model results. The method used by Li et al. (2009) is adopted to test the influence of Tibetan rivers on model results by assuming that the contribution of Tibetan rivers to global weathering flux increased linearly from zero to the present value since 40 Ma. Two scenarios are used (Test runs #1 & #2). Test run #1 assumes that carbonate weathering is responsible for the high $^{87}Sr/^{86}Sr$ ratio of Tibetan rivers, thus the global mean $^{87}Sr/^{86}Sr$ ratio of carbonate weathering will increase from 0.7077 to 0.7081 over the last 40 Ma (Li et al., 2009). Test run #2 assumes that the high $^{87}Sr/^{86}Sr$ ratio of Tibetan rivers is solely contributed by silicate weathering, thus the global mean $^{87}Sr/^{86}Sr$ ratio of silicate weathering will be reduced to 0.7193 before 40 Ma (Li et al., 2009). Both scenarios have similar and very small effects on the model results (Fig. 2). The sensitive tests seem to contradict other models (e.g., Goddéris and François, 1995; Francois and Goddéris, 1998) that have shown the change in Himalayan riverine flux was important for Sr isotopic evolution of seawater and Sr isotopic record of seawater could not be used to reconstruct silicate weathering flux. The reason behind is that not only Himalayan rivers but also other rivers (with less radiogenic $^{87}Sr/^{86}Sr$ ratio) leading out Tibetan Plateau are concerned in this model. Thus, the overall $^{87}Sr/^{86}Sr$ ratio of Tibetan rivers (0.71448) is close to that of global average (0.7116), and its influence on model results is reduced.

Model doesn't separate basalt in continent from other silicate rocks, while the weathering rate of continental basalt may have markedly different response to temperature, runoff and tectonic uplift compared to other silicate rocks in continents. Test run #3 is performed assuming that weathering of continental basalt act as the same as island basalt. A value of 2×10^{12} mol/year is given to the CO_2 consumption of basalt weathering in continents (Dessert et al., 2003). The CO_2 consumption as well as the Sr and Os released by basalt weathering in continents could thus be incorporated into island basalt weathering in the test run. Corresponding changes of the primary parameters are listed in Table 4. The results show that test run #3 has very small influence on the model results except for the weathering of island basalt (Fig. 2). The relative rate of island basalt weathering show smaller amplitude of changes with evolving shape unaltered. The reduced amplitude of changes is caused by higher late Pleistocene flux of island basalt weathering in the test run #3 (Table 4).

3. RESULTS AND VALIDATION

Fig. 2 shows the reconstructed key fluxes of carbon cycle. Although differing from each other in details and amplitudes of variation, weathering of continental rocks and burial of carbonate and organic carbon share a very similar trend over the past 100 million years. They all show a relatively high value during the Late Cretaceous. After holding a minimum in Paleocene, they gradually increased toward the high fluxes of Late Pleistocene. Unlike these similar patterns is weathering of island basalt, which has experienced a progressive decrease since 100 Ma.

Since all of the model results are calculated simultaneously from the same set of equations, the consistence between the model results and geological records could help check veracities of the model. The reconstructed burial rate of carbonate generally agree with that integrated from the world's ocean basins except for the 40–60 Ma portion (Fig. 2d). The model shows a significant underestimation of the carbonate deposition flux for the period 40–60 Ma compared to the reconstruction by Opdyke and Wilkinson (1988) while the model of François and Goddéris (Francois

Table 2
Primary parameters used in the model.

No.	Symbol	Description	Value[a]	Error	References
1	C_{carbw}	Carbonate weathering	12.3×10^{12} mol/year	×5%	Gaillardet et al. (1999)
2	C_{ma}	CO_2 degassing from mid-ocean ridge and arc	4.7×10^{12} mol/year	×5%	Marty and Tolstikhin (1998)
3	C_{volc}	Volcanic CO_2 degassing	6.0×10^{12} mol/year	×5%	Marty and Tolstikhin (1998)
4	Δ	$\delta^{13}C$ difference between sedimentary carbonate and organic C	30‰	0.5‰	Hayes et al. (1999)
5	$\delta^{13}C_{carbw}$	Average $\delta^{13}C$ of carbonate rocks	1.8‰	0.1‰	Derry and France-Lanord (1996)
6	$\delta^{13}C_{volc}$	$\delta^{13}C$ of volcanic CO2	−5.0‰	0.1‰	Derry and France-Lanord (1996)
7	$\delta^{13}C_{carbb}$	$\delta^{13}C$ of marine carbonate	Fig. 1b	0.2‰	Falkowski et al. (2005)
8	$\delta^{13}C_{orgb}$	$\delta^{13}C$ of marine organic C	Fig. 1c	0.5‰	Falkowski et al. (2005)
9	A_{siliw}	Bicarbonate production of continental silicate weathering	8.7×10^{12} mol/year	×5%	Gaillardet et al. (1999)
10	A_{basw}	Bicarbonate production of island basalt weathering	5.0×10^{12} mol/year	×5%	b
11	N	Amount of Sr in seawater	1.25×10^{17} mol	×50%	Palmer and Edmond (1989)
12	S_{rw}	Strontium flux of continental weathering	3.4×10^{10} mol/year	×5%	Davis et al. (2003)
13	S_{rdia}	Diagenetic Sr product	3.4×10^{9} mol/year	×20%	Elderfield and Gieskes (1982)
14	f_{csiliw}	Fraction of silicate weathering Sr in Srw	31%	×50%	Gaillardet et al. (1999)
15	f_{basw}	Fraction of basalt weathering Sr in hydrothermal and basalt weathering Sr flux	73%	×10%	Allègre et al. (2010)
16	$^{87}Sr/^{86}S_{rw}$	$^{87}Sr/^{86}Sr$ of continental weathering	0.7116	0.0002	Davis et al. (2003)
17	$^{87}Sr/^{86}S_{rcarbw}$	$^{87}Sr/^{86}Sr$ of carbonate weathering	0.7077	0.0002	Li et al. (2009)
18	$^{87}Sr/^{86}S_{rmantle}$	$^{87}Sr/^{86}Sr$ of hydrothermal output and basalt weathering similar to mantle value	0.7037	0.0002	Bach and Humphris (1999)
19	$^{87}Sr/^{87}S_{rdia}$	$^{87}Sr/^{86}Sr$ of diagenetic Sr product	0.7084	0.001	Elderfield and Gieskes (1982)
20	$^{87}Sr/^{86}S_{\mathrm{rocean}}$	$^{87}Sr/^{86}Sr$ of seawater	Fig. 1d	0.00002	Mcarthur et al. (2001)
21	Os/S_w	Os/SO_4^{2-} ratio of sediment weathering	0.34 × 10−9	×20%	Li et al. (2009)
22	Os/Si_w	Os/Si ratio of silicate weathering	0.12 × 10−9	×20%	Li et al. (2009)
23	S_w	Riverine SO_4^{2-} flux	3.3×10^{12} mol/year	×20%	Meybeck (2003)
24	S_{iw}	Riverine Si flux	4.7×10^{12} mol/year	×20%	Gaillardet et al. (1999)
25	Os/Sr_{basw}	Os/Sr ratio of basalt weathering	0.61×10^{-9}	×5%	c
26	f_{cos}	Cosmic contribution in basalt weathering, hydrothermal, and cosmic Os flux	0.14	×50%	Levasseur et al. (1999)
27	$^{187}Os/^{188}O_{sw}$	$^{187}Os/^{188}Os$ of continental weathering	1.54	0.05	Levasseur et al. (1999)
28	$^{187}Os/^{188}Os_{csiliw}$	$^{187}Os/^{188}Os$ of continental silicate weathering	1.05	0.2	Peucker-Ehrenbrink and Jahn (2001)
29	$^{187}Os/^{188}Os_{mantle}$	$^{187}Os/^{188}Os$ of hydrothermal, cosmic and basalt weathering Os flux similar to mantle value	0.126	0.05	Allègre and Luck (1980)
30	$^{187}Os/^{188}Os_{ocean}$	$^{187}Os/^{188}Os$ of seawater	Fig. 1e	0.05	Nielsen et al. (2009)
31	Sp	Sea floor spreading rate	Fig. 1a	×2%	Muller et al. (2008)
32	V	Volume of seawater	1.37×10^{21}/L	×20%	
33	$CMg0$	Modern Mg concentration of seawater	54.4 mmol/L	×5%	
34	$CMgi$	Initial Mg concentration of seawater at ~100 Ma	34 mmol/L	×20%	Timofeeff et al. (2006)
35	Mgw	Mg flux of continental weathering	5.5×10^{12} mol/year	×5%	Gaillardet et al. (1999)
36	MgC_{csiliw}	Mg/HCO_3^- ratio of continental silicate weathering	0.13 mol/mol	×20%	Gaillardet et al. (1999)
37	MgC_{basw}	Mg/HCO_3^- ratio of island basalt weathering	0.19 mol/mol	×5%	Dessert et al. (2003)

[a] All are the late Pleistocene values except for the isotopic curves and the spreading rate of sea floor.
[b] Based on the updated bicarbonate production rate of island basalt weathering (2.47×10^6 mol km^{-2} year^{-1}) (Dessert et al., 2003) and the cumulative surface area of basaltic island (2.02×10^6 km^2) (Allègre et al., 2010).
[c] Assuming congruent release of Sr and Os during island basalt weathering and average basalt Os and Sr concentration of 60 ppt and 450 ppm respectively.

Table 3
Parameters used in Eqs. (6)–(12).

Symbol	Description	Value[a]	Notes
C_{carbw}	Carbonate weathering	12.3×10^{12} mol/year	b
C_{orgw}	Organic C weathering	3.6×10^{12} mol/year	c
C_{ma}	CO_2 degassing from mid-ocean ridge and arc	4.7×10^{12} mol/year	b
C_{plume}	Plume CO_2 degassing	1.3×10^{12} mol/year	$C_{volc}-C_{ma}$
C_{carbb}	Carbonate burial	16.8×10^{12} mol/year	d
C_{orgb}	Burial of organic C	5.1×10^{12} mol/year	d
$\delta^{13}C_{carbw}$	δ^{13}C of sedimentary carbonate	1.8‰	b
$\delta^{13}C_{orgw}$	δ^{13}C of sedimentary organic carbon	−28.2‰	$\delta^{13}C_{carbw}-\Delta$
$\delta^{13}C_{ma}$	δ^{13}C of mid-ocean ridge and arc degassing ($\delta^{13}C_{volc}$)	−5.0‰	b
$\delta^{13}C_{plume}$	δ^{13}C of plume degassing ($\delta^{13}C_{volc}$)	−5.0‰	b
$\delta^{13}C_{carbb}$	δ^{13}C of marine carbonate	Fig. 1b	b
$\delta^{13}C_{orgb}$	δ^{13}C of marine organic C	Fig. 1c	b
A_{csiliw}	Bicarbonate production of continental silicate weathering	8.7×10^{12} mol/year	b
A_{basw}	Bicarbonate production of island basalt weathering	5.0×10^{12} mol/year	b
A_{carbw}	Bicarbonate production of carbonate weathering	24.6×10^{12} mol/year	$2 \times C_{carbw}$
A_{carbb}	Bicarbonate consumption of carbonate burial	33.7×10^{12} mol/year	$2 \times C_{carbb}$
A_{rev}	Bicarbonate consumed by reverse weathering	4.6×10^{12} mol/year	d
N	Amount of Sr in seawater	1.25×10^{17} mol	b
$^{87}Sr/^{86}Sr_{ocean}$	^{87}Sr/^{86}Sr of seawater	Fig. 1d	b
Sr_{csiliw}	Sr flux of continental silicate weathering	1.05×10^{10} mol/year	$Sr_w \times f_{csiliw}$
Sr_{carbw}	Sr flux of carbonate weathering	2.35×10^{10} mol/year	Sr_w-Sr_{csiliw}
Sr_{basw}	Island basalt weathering Sr flux	1.07×10^{10} mol/year	e
Sr_{hy}	Hydrothermal Sr flux	0.39×10^{10} mol/year	e
Sr_{dia}	Diagenetic Sr product	3.4×10^{9} mol/year	b
$^{87}Sr/^{86}Sr_{csiliw}$	^{87}Sr/^{86}Sr of continental silicate weathering	0.7203	f
$^{Sr}R_{carbw}$	^{87}Sr/^{86}Sr of carbonate weathering	0.7077	b
$^{87}Sr/^{86}Sr_{basw}$	^{87}Sr/^{86}Sr of basalt weathering ($^{87}Sr/^{86}Sr_{mantle}$)	0.7037	b
$^{87}Sr/^{86}Sr_{hy}$	^{87}Sr/^{86}Sr of hydrothermal output ($^{87}Sr/^{86}Sr_{mantle}$)	0.7037	b
$^{Sr}R_{dia}$	^{87}Sr/^{86}Sr of diagenetic Sr product	0.7084	b
Os_{csiliw}	Os flux of continental silicate weathering	551 mol/year	g
Os_{sediw}	Os flux of sediment weathering	1119 mol/year	g
Os_{basw}	Basalt weathering Os flux	654 mol/year	h
Os_{hy}	Hydrothermal Os flux	56 mol/year	i
Os_{cos}	Cosmic Os flux	115 mol/year	i
$^{187}Os/^{188}Os_{ocean}$	^{187}Os/^{188}Os of seawater	Fig. 1e	b
$^{187}Os/^{188}Os_{csiliw}$	^{187}Os/^{188}Os of continental silicate weathering	1.05	b
$^{Os}R_{sediw}$	^{187}Os/^{188}Os of sediment weathering	1.78	j
$^{187}Os/^{188}Os_{basw}$	^{187}Os/^{188}Os of basalt weathering ($^{187}Os/^{188}Os_{mantle}$)	0.126	b
$^{187}Os/^{188}Os_{hy}$	^{187}Os/^{188}Os of hydrothermal flux ($^{187}Os/^{188}Os_{mantle}$)	0.126	b
$^{187}Os/^{188}Os_{cos}$	^{187}Os/^{188}Os of cosmic flux ($^{187}Os/^{188}Os_{mantle}$)	0.126	b
Sp	Spreading rate of sea floor	Fig. 1a	b
K_{ma}	Mid-ocean and arc degassing proportional to Sp	Fig. 1a	b
K_{hy}	Hydrothermal activity proportional to Sp	Fig. 1a	b
V	Volume of seawater	1.37×10^{21}/L	b
CMg_0	Mg concentration of modern seawater	54.4 mmol/L	b
CMg_i	Initial Mg concentration of seawater	34 mmol/L	b
Mg_{csiliw}	Mg flux of continental silicate weathering	1.2×10^{12} mol/year	$MgC_{csiliw} \times A_{csiliw}$
Mg_{carbw}	Mg flux of carbonate weathering	4.4×10^{12} mol/year	Mg_w-Mg_{csiliw}
Mg_{basw}	Mg flux of island basalt weathering	0.94×10^{12} mol/year	$MgC_{basw} \times A_{basw}$
Mg_{hy}	Hydrothermal Mg sink	4.2×10^{12} mol/year	k

[a] All are the late Pleistocene values except for the isotopic curves and the spreading rate of sea floor.
[b] Same value as in Table 2.
[c] Calculated from the δ^{13}C of bulk earth ($\delta^{13}C_{volc}$), δ^{13}C of average carbonate ($\delta^{13}C_{carbw}$), and average δ^{13}C difference between sedimentary carbonate and organic carbon (δ) after Li et al. (2009).
[d] Derived from Eqs. (6)–(8) under Pleistocene condition when all of the K values equal to 1.
[e] The sum of hydrothermal and basalt weathering Sr flux could be calculated based on Eq. (9) under late Pleistocene configuration that all of the K values equal to 1, of which 73% (f_{basw}) derived from basalt weathering according to Allègre et al. (2010).
[f] Calculated from the ^{87}Sr/^{86}Sr ratio continental riverine Sr flux ($^{87}Sr/^{86}Sr_w$), ^{87}Sr/^{86}Sr ratio of carbonate weathering ($^{87}Sr/^{86}Sr_{carbw}$), and the relative proportion Sr derived from silicate weathering (Sr_{csiliw}) and carbonate weathering (Sr_{carbw}) after Li et al. (2009).

[g] According to Li et al. (2009), Os flux of continental silicate weathering could be calculated from the purely silicate weathering derived riverine Si flux (Si_w) and Os/Si ratio of continental silicate weathering (Os/Si_w). The Os flux of sediment weathering could be calculated from the purely sediment weathering derived riverine SO_4^{2-} flux (S_w) and Os/SO_4^{2-} ratio of sediment weathering (Os/S_w).
[h] Calculated from the Sr flux (Sr_{basw}) and Os/Sr ratio (Os/Sr_{basw}) of basalt weathering.
[i] The sum of hydrothermal, cosmic and basalt weathering Os flux could be calculated based on Eq. (9) under late Pleistocene configuration that all of the K values equal to 1, of which 14% (f_{cos}) derived from cosmic flux according to Levasseur et al. (1999). Hydrothermal Os flux is then calculated by subtract the basalt weathering Os flux (Os_{basw}) from the rest of the 86% Os flux.
[j] Calculated from the $^{187}Os/^{188}Os$ ratio of continental riverine Os ($^{187}Os/^{188}O_{sw}$), $^{187}Os/^{188}Os$ ratio of continental silicate weathering ($^{187}Os/^{188}Os_{csiliw}$), and the relative proportion of Os derived from silicate weathering (Os_{csiliw}) and sediment weathering (Os_{sediw}) after Li et al. (2009).
[k] Value is tuned in the model so that the resulting Mg concentration of modern ocean could matches the observation.

and Goddéris, 1998) show much less discrepancy in their reconstruction for this period. The reason behind this discrepancy is not clear. The model results indicate that the low value of carbonate deposition between the 60–40 Ma window is caused by low weathering flux of carbonate rock (Fig. 2b and d). It is the weathering of carbonate rock that dominates the alkalinity flux (Table 3), and thus controls the carbonate deposition. However, the reconstruction of carbonate sedimentation, either by model or basin integration, is more accurate on the relative variation in short-term than the long-term trend and absolute value. Notably, the model has successfully captured the major shifts of the carbonate burial reconstructed by basin integration (Fig. 2d). Model validation could also be made on the concentration of Mg in seawater. The modeled concentration of Mg in seawater shows a dramatic increase during the course of Cenozoic (Fig. 2f), which is consistent with the observation based on fluid inclusion (Zimmermann, 2000; Horita et al., 2002; Timofeeff et al., 2006).

4. DISSCUSSION

4.1. Roles of physical erosion

The similar trends shared by weathering of continental rocks and burial of carbonate and organic carbon suggests a common control behind (Fig. 2). Factors that control rock weathering are very complex but are normally related to exposure area of rocks, rate of physical erosion and climate condition. Under weathering limited regime, weathering reaction is promoted under higher temperature and runoff. However, the Cenozoic increase in continental weathering is in the opposite of global climate change. Decreasing sea level associated with Cenozoic glaciation may increase exposure area of continents by several percents, which is still too small to explain the dramatic increase in weathering product unless low lands are characterized by extremely high weathering flux. Weathering of continental rocks seems to be highly correlated with the rate of physical erosion as reflected by global production of terrigenous sediment (Figs. 2 and 4), supporting a supply limited weathering regime for continental rocks. As proposed by Raymo and Ruddiman (1992), increase of physical erosion might be related to the widespread mountain building during the Cenozoic. However, taken at face value, the correlation between the sediment discharge (Fig. 2b) and continental silicate weathering is not very good in detail. This is because the relationship between physical erosion (sediment yield) and silicate weathering is non-linear (Fig. 4).

Sedimentation rate of carbonate mimics carbonate weathering largely because carbonate weathering is the major supplier of alkalinity to the ocean while carbonate burial is the dominant sink of alkalinity. Ocean could maintain a quasistatic equilibrium of alkalinity automatically simply by changing alkalinity and thus carbonate compensation depth and the efficiency of carbonate preservation (Broecker and Peng, 1982). The way that the burial of organic carbon follows continental weathering may also be modulated by physical erosion. Processes that control production and preservation of particulate organic matter are very complex. Increasing supply of nutrient such as phosphorus from continental weathering may promote primary productivity in the ocean. However, more than 99% of sinking particles are oxidized in the water column of ocean. A slight shift in the efficiency of oxidation, say a drop to 98%, would double the preservation. Late Cenozoic cooling and increasing meridional temperature gradient may facilitate the formation of oxygen-rich deep water, a condition that may not be favored for the survival of organic matter through water column. Once settled in sediment, organic matter also subjects to further oxidation. Only a small fraction of organic particle could survive at this stage. It is shown that preservation of organic matter is largely elevated under high sedimentation rate (France-Lanord and Derry, 1997). As a matter of fact, the majority of organic carbon buried today takes places in shallow marine environments with high debris flux such estuaries, continental shelves and deltas (Berner and Canfield, 1989). In these well-oxygenated environments, burial rate of organic carbon is a positive function of total sedimentation rate (Stein, 1990). Late Cenozoic increase in physical erosion, and thus sediment production may have increased the burial of organic matter.

4.2. Implication for pCO_2

Carbon dioxide in the ocean–atmosphere system is mainly derived from volcanic degassing, oxidation of organic matter, and reverse weathering (include bicarbonate neutralized by hydrothermal H^+ inputs). Silicate weathering and burial of organic matters remove CO_2 from the ocean–atmosphere system. Carbonate weathering cannot serve as a long-term sink for atmospheric CO_2 since the

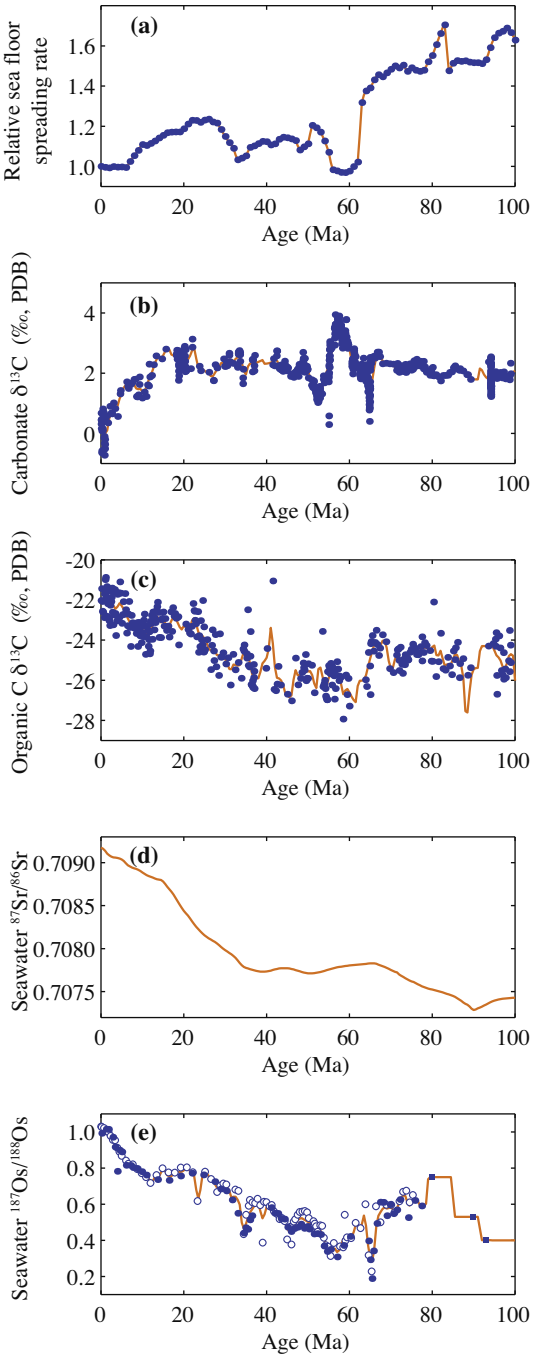

Fig. 1. Model constrains. (a) Spreading rate of mid-ocean ridge (Muller et al., 2008). (b and c) $\delta^{13}C$ of marine carbonate and organic carbon (Falkowski et al., 2005). (d) Strontium isotopic composition of seawater from updated LOWESS database (Mcarthur et al., 2001). (e) Osmium isotopic composition of seawater. The <80 Ma portion is compiled from records of two ferromanganese crusts, D11 (open circle) (Klemm et al., 2005) and CD29 (dots) (Burton, 2006), based on the Re decay correction and age calibration of Nielsen et al. (2009). The >80 Ma portion (square) is compiled from the other sources (Peucker-Ehrenbrink et al., 1995; Cohen et al., 1999; Ravizza et al., 1999). Model uses the smoothed fits to the raw data.

same amount of CO_2 absorbed by carbonate weathering will be released subsequently by carbonate sedimentation. Mathematically, mass balance of CO_2 in the ocean–atmosphere system could be deduced by canceling the carbonate terms in Eqs. (6) and (8) since every 2 mol of alkalinity is associated with 1 mol of CO_2 during weathering and burial of carbonate, i.e., $A_{carbw} = 2 \times C_{carbw}$, $A_{carbb} = 2 \times C_{carbb}$:

$$\sum(K_i \times C_i) = \sum(K_j \times C_j) \tag{15}$$

where subscripts i includes *orgw* (weathering of organic carbon), *ma* (CO_2 degassing from mid-ocean ridge and arc volcanoes), *plume* (plume CO_2 degassing) and *rev* (reverse weathering plus neutralization of bicarbonate by hydrothermal H^+); subscripts j includes *csiliw* (continental silicate weathering), *basw* (weathering of island basalt), and *orgb* (burial of organic carbon); $C_{rev} = A_{rev}/2$; $C_{csiliw} = A_{csiliw}/2$; $C_{basw} = A_{basw}/2$. The calculated source and sinks of CO_2 over the past 100 million years are shown in Fig. 5.

The limited reservoir of CO_2 in ocean and atmosphere imply that all sources and sinks of CO_2 must be in a perfect balance on time scale of million years (Berner et al., 1983). Any imbalance of CO_2 budget will result in dramatic change of pCO_2 in a short time. Mass balance of atmospheric CO_2 could be maintained automatically if any sources or sinks of CO_2 is sensitive to pCO_2 or the pCO_2 controlled environmental factors, and thus provide a negative feedback loop between pCO_2 and the CO_2 sources or sinks. Volcanic degassing and hydrothermal activity is related to the internal processes of the earth, which is unlikely modulated by the changes of surface environment. Continental silicate weathering and the cycling of organic carbon seem to be largely controlled by physically erosion. They may not serve as negative feedback to pCO_2 unless physical erosion is in some way promoted under high level of pCO_2.

The general decreasing trend of pCO_2 and temperature over the past 100 million years (Fig. 6) imply that the pCO_2-sensitive CO_2 flux should increase if it act as a CO_2 source or decrease as a CO_2 sink. Weathering of island basalt matches such a criteria (Fig. 6). Due to strong physical erosion in oceanic islands (Milliman and Meade, 1993), weathering of island basalt may be largely weathering limited, and thus is very sensitive to pCO_2 or the pCO_2 controlled environmental factors. However, resolving the mechanisms behind the negative feedbacks between basalt weathering and pCO_2 is not straightforward. Basalt weathering may response directly to pCO_2 through the fertilization of CO_2 on terrestrial biomass and thus plant weathering. Terrestrial plants take up CO_2 primarily by diffusion. Increasing pCO_2 generally has positive effect on photosynthesis, productivity, growth, and root activity, which accelerate plant weathering (Andrews and Schlesinger, 2001; Ainsworth and Long, 2005; Baars et al., 2008). Previous model of carbon cycle indicates that the efficiency of CO_2 fertilization on terrestrial plants is a key factor controlling the long-term evolution of pCO_2 models (Berner and Kothavala, 2001). Rising of vascular plant in Silurian and subsequently expansion in Devonian have caused a major drawdown of pCO_2 (Berner, 1997).

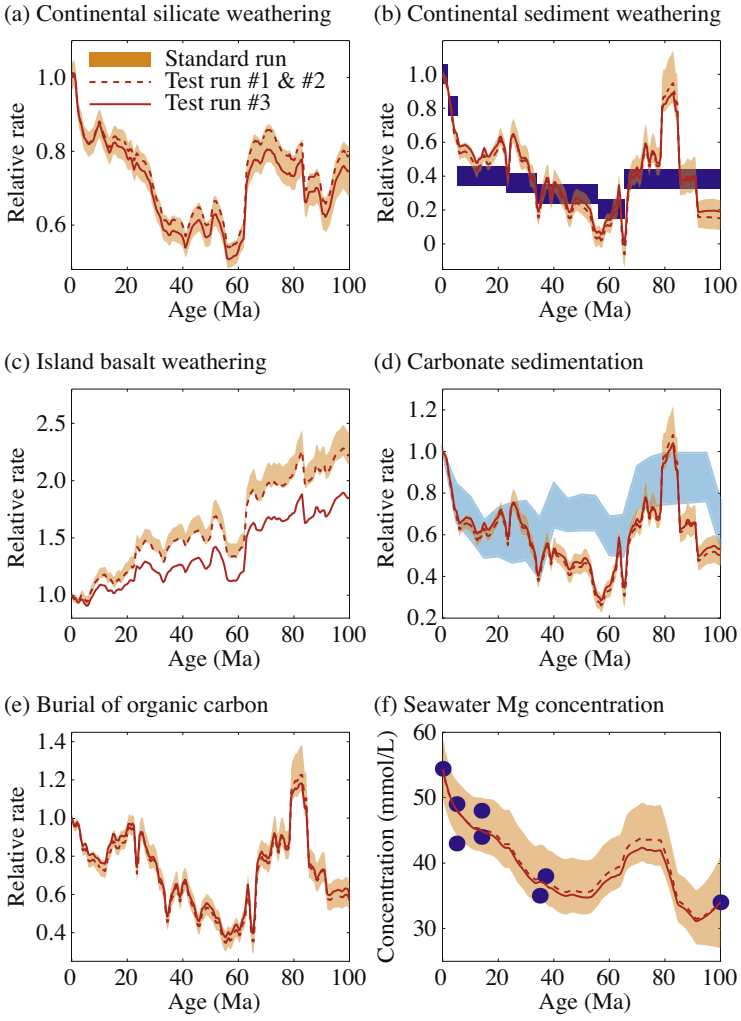

Fig. 2. Model results. (a–e) Relative rates of continental silicate weathering, weathering of sedimentary rocks, island basalt weathering, carbonate sedimentation and burial organic C. (f) Mg concentration of seawater. Shaded envelopes are accumulative errors of the model. Test runs #1 & #2 indicate the influence of changing contribution of Tibetan rivers since 40 Ma. Test run #3 treats weathering of continental basalt as island basalt. Also shown are the relative rate of physical erosion (blue bars, Fig. 2b) reconstructed from global terrigenous sediment production (Hay et al., 2006), relative carbonate sedimentation rate (cyan shade area, Fig. 2d) integrated from worldwide ocean basins (Opdyke and Wilkinson, 1988), and Mg concentration of seawater (blue dots, Fig. 2f) reconstructed from halite inclusion (Zimmermann, 2000; Horita et al., 2002; Timofeeff et al., 2006). (For interpretation of the references to color in this figure legend, the reader is referred to the web version of this article.)

The continuous decrease of basalt weathering over the past 100 million years shows good coherence with the global cooling as reflected by oxygen isotope of benthic foraminifera (Fig. 6). It is generally accepted that mineral dissolution mediated by temperature or runoff act as the key mechanism in the negative feedbacks between pCO_2 and silicate weathering (Berner et al., 1983). Higher pCO_2 is normally accompanied with higher temperature and runoff through greenhouse effect, and thus higher rate of silicate weathering. Taking an apparent activation energy of about 42 kJ/mol for basalt weathering (Dessert et al., 2001), a 56% drop of basalt weathering since 100 Ma require a temperature cooling of about 12 °C, which might be plausible considering the extremely warm climate of the Late Cretaceous (Bice et al., 2006). As shown by Dessert et al. (2003), the rate of basalt weathering is also a strong function of runoff. Neglecting the effect of temperature, this would imply a huge drop in runoff, which is unlikely to have occurred (Donnadieu et al., 2006). A realistic combination of runoff and temperature reduction might also account for such a large decrease in weathering of island arc.

Determining the coupling between pCO_2 and weathering of island basalt is difficult. Uncertainties of pCO_2 reconstruction are large (Fig. 6). Different proxies usually produce contradict results (Fig. 6). However, if we take the confidence of the proxy-based pCO_2 in an order of phytoplankton $\delta^{13}C$, stomatal indexes, boron isotope, paleosol, a rough trend of pCO_2 could be reconstructed (Fig. 6). Late Cretaceous and Early Cenozoic are characterized by high and variable pCO_2. The pCO_2 decreased rapidly during

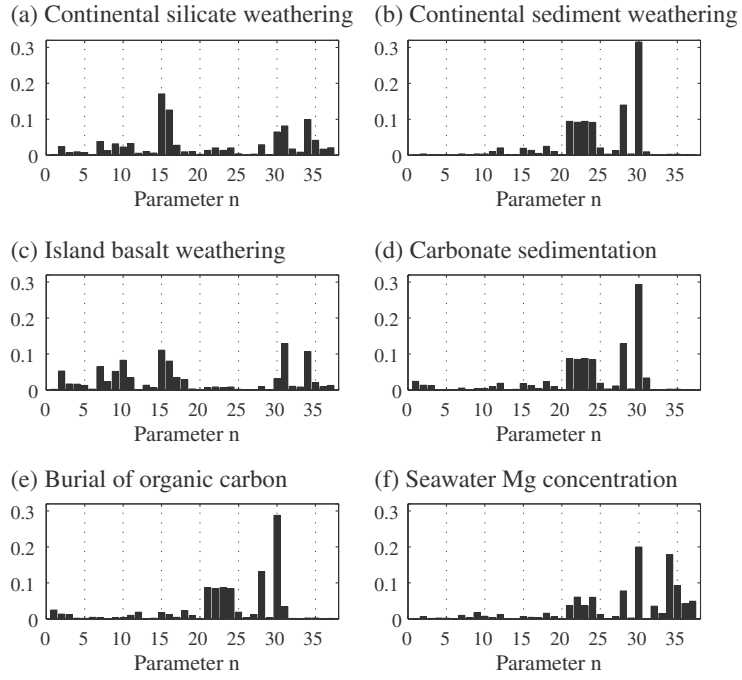

Fig. 3. Error contributions of the primary parameters to the modeled results. Index number of the parameters is listed in Table 2.

Table 4
Changes of primary parameters in test run #3.

Symbol	Description	Standard run	Test run #3[a]
A_{siliw}	Bicarbonate production of continental silicate weathering	8.7×10^{12} mol/year	6.7×10^{12} mol/year
A_{basw}	Bicarbonate production of island basalt weathering	5.0×10^{12} mol/year	7.0×10^{12} mol/year
Sr_w	Strontium flux of continental weathering	3.4×10^{10} mol/year	3.0×10^{10} mol/year
f_{csiliw}	Fraction of silicate weathering Sr in Sr_w	31%	21%
f_{basw}	Fraction of basalt weathering Sr in hydrothermal and basalt weathering Sr flux	73%	79%
$^{87}Sr/^{86}Sr_w$	$^{87}Sr/^{86}Sr$ of continental weathering	0.7116	0.7127
$^{187}Os/^{188}Os_w$	$^{187}Os/^{188}Os$ of continental weathering	1.54	1.80
Mg_w	Mg flux of continental weathering	5.5×10^{12} mol/year	5.2×10^{12} mol/year

[a] Calculated by incorporating the weathering of continental basalt, which consumes about 2.0×10^{12} mol CO_2 per year, into weathering of island.

the Oligocene and then held a low and relatively stable value afterward. It is worthy to notice that the rough trend of pCO_2 does not match the weathering of island basalt perfectly (Fig. 6). Global climate is not the sole function of pCO_2. Other factors, such as land-sea distribution and ocean circulation, also contribute (Kennett, 1977; Scher and Martin, 2006). Thus, pCO_2 may change only when climate condition cannot support a basalt weathering flux that is needed to balance the carbon cycle. A recent finding at the Eocene–Oligocene boundary may be a good example (Pearson et al., 2009). Antarctic glaciation at the Eocene–Oligocene boundary, which is possibly induced by change of ocean circulation (Kennett, 1977), was associated with an increase of pCO_2 afterward (Pearson et al., 2009) to compensate the unsupported basalt weathering flux.

4.3. Evidence from $^{10}Be/^{9}Be$ ratio?

Recently, Willenbring and von Blanckenburg (2010) argued a long-term stability of late Cenozoic global weathering rates mainly based on the nearly constant initial $^{10}Be/^{9}Be$ ratio of seawater. Assuming a constant production of cosmogenic ^{10}Be, the constant initial $^{10}Be/^{9}Be$ ratio of seawater could thus be taken as evidence for constant weathering release of ^{9}Be. Our model results indicate that the late Cenozoic increase of CO_2 consumption by continental silicate weathering has been largely compensated by decreasing weathering of island basalt (Fig. 5). It is not surprising that the total silicate weathering (continental + island basalt) remains roughly constant. Because of mass balance consideration, it must roughly follow the

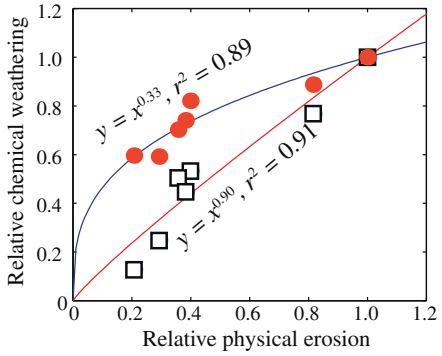

Fig. 4. Correlation between the relative rates of physical erosion and chemical weathering of continental silicate (red dots) and between the relative rates of physical erosion and chemical weathering of sedimentary rocks (black squares). Relative rates of chemical weathering is averaged based on the time period of the physical erosion data in Fig. 2b. (For interpretation of the references to color in this figure legend, the reader is referred to the web version of this article.)

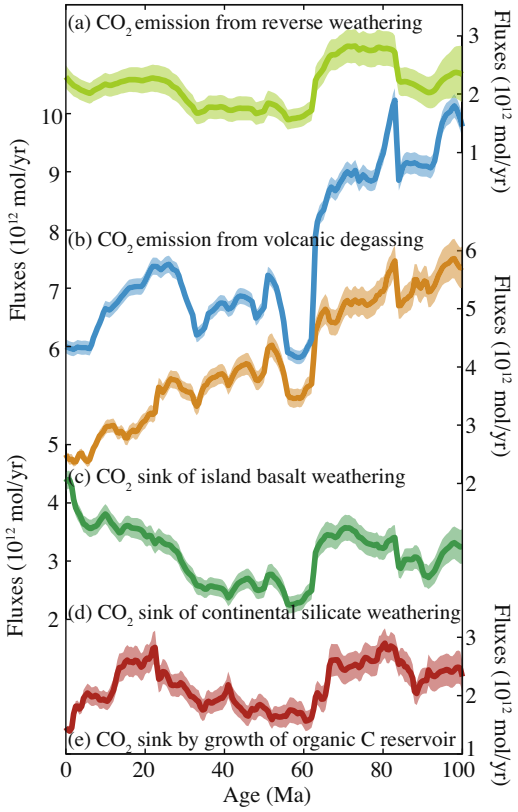

Fig. 5. Balance of CO_2 in atmosphere–ocean system over the past 100 million years. Growth of organic reservoir is calculated by subtracting weathering of organic carbon from organic burial. Note that the scales for CO_2 flux are the same for every panel.

degassing rate, which is rather constant after 60 Ma (Fig. 5b). Decreasing release of ^{9}Be from basalt weathering may have also compensated the increasing ^{9}Be flux of continental weathering. Thus, the constant initial ^{10}Be/^{9}Be

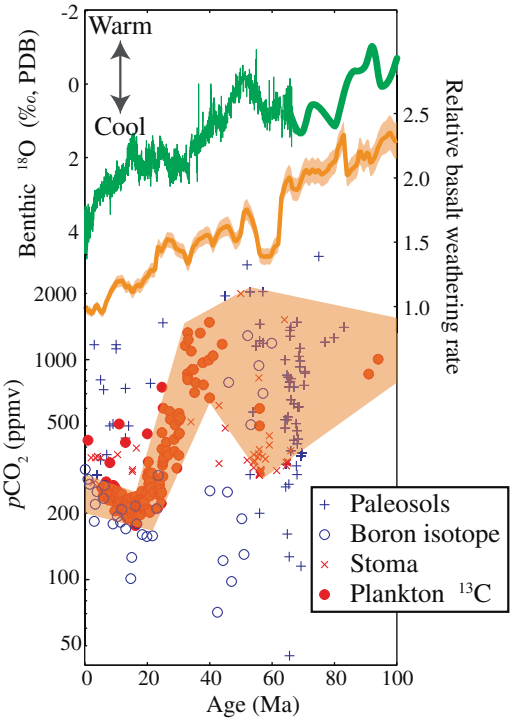

Fig. 6. Evolution of basalt weathering, pCO_2 and global climate. Atmospheric pCO_2 is based on data compilation of Royer (2006). Global climate is indicated by oxygen isotopic record of benthic foraminifera which reflecting the changes of deep sea temperature and/or global ice volume (Zachos et al., 2008; Friedrich et al., 2012).

ratio of seawater may not necessarily invoke a constant continental weathering, but can serve as supporting evidences for the seesaw feedback between weathering of continental silicate and island basalt.

4.4. Implication for seawater Mg concentration

Increasing Mg concentration and thus Mg/Ca ratio of seawater is one of the most prominent changes of oceanic geochemistry over the past 100 million years. Crystalline phase of $CaCO_3$, calcite or aragonite, precipitated from surface ocean largely depends on the Mg/Ca ratio of seawater. Aragonite is the main precipitates of $CaCO_3$ since about 40 Ma due to the increasing Mg/Ca ratio of seawater (Hardie, 1996; Lowenstein et al., 2001). However, the reason behind the increasing Mg/Ca ratio of seawater is still under debates (Coggon et al., 2010; Broecker and Yu, 2011). The consistence between modeled Mg concentration of seawater and that reconstructed from fluid inclusion may provides clues to resolve the processes that modulate the secular variations of Mg concentration and thus Mg/Ca ratio of seawater. The modeled increasing Mg concentration of seawater is largely driven by increasing weathering of carbonate (Fig. 2) since carbonate weathering is the most important Mg source to the ocean (Table 3). Contribution of decreasing spreading rate of sea floor and thus hydrothermal activity is very small since increasing Mg

concentration of seawater has largely compensated the hydrothermal sink of Mg.

One may argue that increasing Mg/Ca ratio of seawater may not favor an increasing weathering of carbonate rock with Mg/Ca ratio much lower than seawater (Coggon et al., 2010). However, Ca released by carbonate weathering will be precipitated rapidly as carbonate due to the instantaneous balance of alkalinity, leaving the Mg in oceans pending for later sink. As formation of dolomite is not widespread during the Cenozoic, the increasing Mg flux associated with carbonate weathering was accumulated in the ocean, which ultimately increases Mg/Ca ratio of seawater.

5. CONCLUSIONS

Reverse calculation based on marine C, Sr and Os isotopic records and spreading rate of sea floor indicates that increasing physical erosion is the most prominent driver for cycling of carbon and Mg over the past 100 million years. Weathering of continental rocks are largely promoted by the increasing physical erosion in response to the widespread mountain building of Cenozoic. Elevated carbonate weathering and thus release of Mg may have contributed to the raising Mg concentration of seawater. Disturbances of atmospheric CO_2 cycle, which are induced either by increasing weathering continental silicate rocks or by the changes of volcanic degassing and growth of organic reservoir, have been balanced by the rapid adjustment of island basalt weathering. The kinetically controlled weathering of island basalt, which is sensitive to pCO_2 or the pCO_2-controlled environmental factors, may have facilitated the rapid adjustment of island basalt weathering to compensate the disturbance of atmospheric CO_2 balance.

ACKNOWLEDGMENTS

China Geological Survey (Shui [2010] Kuangping 03-07-08) and National Science Foundation of China (41173105, 41102103 and 41021002) supported this work. This work was funded in part by The European Research Council (ERC grant 2010-NEWLOG ADG-267931 HE).

REFERENCES

Ainsworth E. A. and Long S. P. (2005) What have we learned from 15 years of free-air CO_2 enrichment (FACE)? A meta-analytic review of the responses of photosynthesis, canopy. *New Phytol.* **165**, 351–371.

Allègre C. J. and Luck J. M. (1980) Osmium isotopes as petrogenetic and geological tracers. *Earth Planet. Sci. Lett.* **48**, 148–154.

Allègre C. J., Louvat P., Gaillardet J., Meynadier L., Rad S. and Capmas F. (2010) The fundamental role of island arc weathering in the oceanic Sr isotope budget. *Earth Planet. Sci. Lett.* **292**, 51–56.

Andrews J. A. and Schlesinger W. H. (2001) Soil CO_2 dynamics, acidification, and chemical weathering in a temperate forest with experimental CO_2 enrichment. *Global Biogeochem. Cycles* **15**, 149–162.

Arvidson R. S., Mackenzie F. T. and Guidry M. (2006) MAGic: a Phanerozoic model for the geochemical cycling of major rock-forming components. *Am. J. Sci.* **306**, 135–190.

Baars C., Jones T. H. and Edwards D. (2008) Microcosm studies of the role of land plants in elevating soil carbon dioxide and chemical weathering. *Global Biogeochem. Cycles* **22**, 9.

Bach W. and Humphris S. E. (1999) Relationship between the Sr and O isotope compositions of hydrothermal fluids and the spreading and magma-supply rates at oceanic spreading centers. *Geology* **27**, 1067–1070.

Berner R. A. (1997) The rise of plants and their effect on weathering and atmospheric CO_2. *Science* **276**, 544–546.

Berner R. A. (2006) Inclusion of the weathering of volcanic rocks in the GEOCARBSULF model. *Am. J. Sci.* **306**.

Berner R. A. and Caldeira K. (1997) The need for mass balance and feedback in the geochemical carbon cycle. *Geology* **25**, 955–956.

Berner R. A. and Canfield D. (1989) A model for atmospheric oxygen over Phanerozoic time. *Am. J. Sci.* **289**, 333–361.

Berner R. A. and Kothavala Z. (2001) Geocarb III: a revised model of atmospheric CO_2 over Phanerozoic time. *Am. J. Sci.* **301**, 182–204.

Berner R. A., Lasaga A. C. and Garrels R. M. (1983) The carbonate–silicate geochemical cycle and its effect on atmospheric carbon dioxide over the past 100 million years. *Am. J. Sci.* **283**, 641–683.

Bice K. L., Birgel D., Meyers P. A., Dahl K. A., Hinrichs K. and Norris R. D. (2006) A multiple proxy and model study of Cretaceous upper ocean temperatures and atmospheric CO_2 concentrations. *Paleoceanography* **21**, PA2002.

Broecker W. and Yu J. (2011) What do we know about the evolution of Mg to Ca ratios in seawater? *Paleoceanography* **26**, PA3203.

Broecker W. S. and Peng T. H. (1982) *Tracers in the Sea*. Eldigio Press, Palisades, NY.

Burton K. W. (2006) Global weathering variations inferred from marine radiogenic isotope records. *J. Geochem. Explor.* **88**, 262–265.

Coggon R. M., Teagle D. A. H., Smith-Duque C. E., Alt J. C. and Cooper M. J. (2010) Reconstructing past seawater Mg/Ca and Sr/Ca from mid-ocean ridge flank calcium carbonate veins. *Science* **327**, 1114–1117.

Cohen A. S., Coe A. L., Bartlett J. M. and Hawkesworth C. J. (1999) Precise Re–Os ages of organic-rich mudrocks and the Os isotope composition of Jurassic seawater. *Earth Planet. Sci. Lett.* **167**, 159–173.

Davis A. C., Bickle M. J. and Teagle D. A. H. (2003) Imbalance in the oceanic strontium budget. *Earth Planet. Sci. Lett.* **211**, 173–187.

DeConto R. M. and Pollard D. (2003) Rapid Cenozoic glaciation of Antarctica induced by declining atmospheric CO_2. *Nature* **421**, 245–249.

Derry L. A. and France-Lanord C. (1996) Neogene growth of the sedimentary organic carbon reservoir. *Paleoceanography* **11**, 267–276.

Dessert C., Dupr B., Francois L. M., Schott J., Gaillardet J., Chakrapani G. and Bajpai S. (2001) Erosion of Deccan Traps determined by river geochemistry: impact on the global climate and the $^{87}Sr/^{86}Sr$ ratio of seawater. *Earth Planet. Sci. Lett.* **188**, 459–474.

Dessert C., Dupr B., Gaillardet J., François L. M. and Allègre C. J. (2003) Basalt weathering laws and the impact of basalt weathering on the global carbon cycle. *Chem. Geol.* **202**, 257–273.

Donnadieu Y., Goddéris Y., Pierrehumbert R., Dromart G., Fluteau F. and Jacob R. (2006) A GEOCLIM simulation of climatic and biogeochemical consequences of Pangea breakup. *Geochem. Geophys. Geosyst.* **7**, Q11019.

Edmond J. M. (1992) Himalayan tectonics, weathering processes, and the strontium isotope record in marine limestones. *Science* **258**, 1594–1597.

Elderfield H. and Gieskes J. M. (1982) Sr isotopes in interstitial waters of marine sediments from Deep Sea Drilling Project cores. *Nature* **300**, 493–497.

Elderfield H. and Schultz A. (1996) Mid-ocean ridge hydrothermal fluxes and the chemical composition of the ocean. *Annu. Rev. Earth Planet. Sci.* **24**, 191–224.

Falkowski P. G., Katz M. E., Milligan A. J., Fennel K., Cramer B. S., Aubry M. P., Berner R. A., Novacek M. J. and Zapol W. M. (2005) The rise of oxygen over the past 205 million years and the evolution of large placental mammals. *Science* **309**, 2202–2204.

France-Lanord C. and Derry L. A. (1997) Organic carbon burial forcing of the carbon cycle from Himalayan erosion. *Nature* **390**, 65–67.

Francois L. M. and Goddéris Y. (1998) Isotopic constraints on the Cenozoic evolution of the carbon cycle. *Chem. Geol.* **145**, 177–212.

Francois L. M. and Walker J. C. G. (1992) Modelling the Phanerozoic carbon cycle and climate; constraints from the $^{87}Sr/^{86}Sr$ isotopic ratio of seawater. *Am. J. Sci.* **292**, 81–135.

Friedrich O., Norris R. D. and Erbacher J. (2012) Evolution of middle to Late Cretaceous oceans, ÄiA 55 m.y. record of Earth's temperature and carbon cycle. *Geology* **40**, 107–110.

Gaillardet J., Dupré B., Louvat P. and Allègre C. J. (1999) Global silicate weathering and CO_2 consumption rates deduced from the chemistry of large rivers. *Chem. Geol.* **159**, 3–30.

Gaillardet J., Rad S., Rivé K., Louvat P., Gorge C., Allègre C. J. and Lajeunesse E. (2011) Orography-driven chemical denudation in the Lesser Antilles: evidence for a new feed-back mechanism stabilizing atmospheric CO2. *Am. J. Sci.* **311**, 851–894.

Galy A., France-Lanord C. and Derry L. A. (1999) The strontium isotopic budget of Himalayan rivers in Nepal and Bangladesh. *Geochim. Cosmochim. Acta* **63**, 1905–1925.

Goddéris Y. and François L. M. (1995) The Cenozoic evolution of the strontium and carbon cycles: relative importance of continental erosion and mantle exchanges. *Chem. Geol.* **126**, 169–190.

Goddéris Y. and François L. M. (1996) Balancing the Cenozoic carbon and alkalinity cycles: constraints from isotopic records. *Geophys. Res. Lett.* **23**, 3743–3746.

Hardie L. A. (1996) Secular variation in seawater chemistry: an explanation for the coupled secular variation in the mineralogies of marine limestones and potash evaporites over the past 600 m.y. *Geology* **24**, 279–283.

Hay W. W., Migdisov A., Balukhovsky A. N., Wold C. N., Flögel S. and Söding E. (2006) Evaporites and the salinity of the ocean during the Phanerozoic: implications for climate, ocean circulation and life. *Palaeogeogr. Palaeoclimatol. Palaeoecol.* **240**, 3–46.

Hay W. W., Sloan J. L. and Wold C. N. (1988) Mass/age distribution and composition of sediments on the ocean floor and the global rate of sediment subduction. *J. Geophys. Res.* **93**, 14933–14940.

Hayes J. M., Strauss H. and Kaufman A. J. (1999) The abundance of ^{13}C in marine organic matter and isotopic fractionation in the global biogeochemical cycle of carbon during the past 800 Ma. *Chem. Geol.* **161**, 103–125.

Hodell D. A., Mueller P. A., McKenzie J. A. and Mead G. A. (1989) Strontium isotope stratigraphy and geochemistry of the late Neogene ocean. *Earth Planet. Sci. Lett.* **92**, 165–178.

Horita J., Zimmermann H. and Holland H. D. (2002) Chemical evolution of seawater during the Phanerozoic: implications from the record of marine evaporites. *Geochim. Cosmochim. Acta* **66**, 3733–3756.

Jacobson A. D. and Blum J. D. (2000) Ca/Sr and Sr-87/Sr-86 geochemistry of disseminated calcite in Himalayan silicate rocks from Nanga Parbat: influence on river-water chemistry. *Geology* **28**, 463–466.

Kashiwagi H., Ogawa Y. and Shikazono N. (2008) Relationship between weathering, mountain uplift, and climate during the Cenozoic as deduced from the global carbon-strontium cycle model. *Palaeogeogr. Palaeoclimatol. Palaeoecol.* **270**, 139–149.

Kennett J. P. (1977) Cenozoic evolution of Antarctic Glaciation, the Circum-Antarctic Ocean, and their impact on global paleoceanography. *J. Geophys. Res.* **82**, 3843–3860.

Klemm V., Levasseur S., Frank M., Hein J. R. and Halliday A. N. (2005) Osmium isotope stratigraphy of a marine ferromanganese crust. *Earth Planet. Sci. Lett.* **238**, 42–48.

Kump L. R. (1989) Alternative modeling approaches to the geochemical cycles of carbon, sulfur, and strontium isotopes. *Am. J. Sci.* **289**, 390–410.

Kump L. R. and Arthur M. A. (1997) Global chemical erosion during the Cenozoic: weatherability balances the budget. In *Tectonics Uplift and Climate Change* (ed. W. Ruddiman). Plenum Publishing Co..

Kump L. R., Brantley S. L. and Arthur M. A. (2000) Chemical, weathering, atmospheric CO_2, and climate. *Annu. Rev. Earth Planet. Sci.* **28**, 611–667.

Levasseur S., Birck J. L. and Allègre C. J. (1999) The osmium riverine flux and the oceanic mass balance of osmium. *Earth Planet. Sci. Lett.* **174**, 7–23.

Li G., Ji J., Chen J. and Kemp D. B. (2009) Evolution of the Cenozoic carbon cycle: the roles of tectonics and CO_2 fertilization. *Global Biogeochem. Cycles* **23**, GB1009. http://dx.doi.org/10.1029/2008GB003220.

Louvat P., Gislason S. R. and Allègre C. J. (2008) Chemical and mechanical erosion rates in Iceland as deduced from river dissolved and solid material. *Am. J. Sci.* **308**, 679–726.

Lowenstein T. K., Timofeeff M. N., Brennan S. T., Hardie L. A. and Demicco R. V. (2001) Oscillations in Phanerozoic seawater chemistry: evidence from fluid inclusions. *Science* **294**, 1086–1088.

Marty B. and Tolstikhin I. N. (1998) CO_2 fluxes from mid-ocean ridges, arcs and plumes. *Chem. Geol.* **145**, 233–248.

McArthur J. M., Howarth R. J. and Bailey T. R. (2001) Strontium isotope stratigraphy: LOWESS version 3: best fit to the marine Sr-isotope curve for 0–509 Ma and accompanying look-up table for deriving numerical age. *J. Geol.* **109**, 155–170.

Meybeck M. (2003) Global occurrence of major elements in rivers. In *Treatise on Geochemistry* (eds. H. D. Holland and K. K. Turekian). Pergamon, Oxford.

Michalopoulos P. and Aller R. C. (1995) Rapid clay mineral formation in Amazon Delta sediments: reverse weathering and oceanic elemental cycles. *Science* **270**, 614–617.

Milliman J. D. and Meade R. H. (1993) World-wide delivery of river sediments to the oceans. *J. Geol.* **91**, 1–21.

Moulton K. L. and Berner R. A. (1998) Quantification of the effect of plants on weathering: studies in Iceland. *Geology* **26**, 895–898.

Muller R. D., Sdrolias M., Gaina C., Steinberger B. and Heine C. (2008) Long-term sea-level fluctuations driven by ocean basin dynamics. *Science* **319**, 1357–1362.

Nielsen S. G., Mar-Gerrison S., Gannoun A., LaRowe D., Klemm V., Halliday A. N., Burton K. W. and Hein J. R. (2009) Thallium isotope evidence for a permanent increase in marine organic carbon export in the early Eocene. *Earth Planet. Sci. Lett.* **278**, 297–307.

Opdyke B. N. and Wilkinson B. H. (1988) Surface area control of shallow cratonic to deep marine carbonate accumulation. *Paleoceanography* **3**, 685–703.

Pagani M., Zachos J. C., Freeman K. H., Tipple B. and Bohaty S. (2005) Marked decline in atmospheric carbon dioxide concentrations during the Paleogene. *Science* **309**, 600–603.

Palmer M. R. and Edmond J. M. (1989) The strontium isotope budget of the modern ocean. *Earth Planet. Sci. Lett.* **92**, 11–26.

Pearson P. N., Foster G. L. and Wade B. S. (2009) Atmospheric carbon dioxide through the Eocene–Oligocene climate transition. *Nature* **461**, 1110–1113.

Pearson P. N. and Palmer M. R. (2000) Atmospheric carbon dioxide concentrations over the past 60 million years. *Nature* **406**, 695–699.

Peucker-Ehrenbrink B. and Jahn B. M. (2001) Rhenium-osmium isotope systematics and platinum group element concentrations: loess and the upper continental crust. *Geochem. Geophys. Geosyst.* **2**, 2001GC000172.

Peucker-Ehrenbrink B., Ravizza G. and Hofmann A. W. (1995) The marine $^{187}Os/^{186}Os$ record of the past 80 million years. *Earth Planet. Sci. Lett.* **130**, 155–167.

Ravizza G., Sherrell R. M., Field M. P. and Pickett E. A. (1999) Geochemistry of the Margi umbers, Cyprus, and the Os isotope composition of Cretaceous seawater. *Geology* **27**, 971–974.

Raymo M. E. (1994) The Himalayas, organic carbon burial, and climate in the Miocene. *Paleoceanography* **9**, 399–404.

Raymo M. E. and Ruddiman W. F. (1992) Tectonic forcing of late Cenozoic climate. *Nature* **359**, 117–122.

Raymo M. E., Ruddiman W. F. and Froelich P. N. (1988) Influence of late Cenozoic mountain building on ocean geochemical cycles. *Geology* **16**, 649–653.

Rowley D. B. (2002) Rate of plate creation and destruction: 180 Ma to present. *Geol. Soc. Am. Bull.* **114**, 927–933.

Royer D. L. (2006) CO_2-forced climate thresholds during the Phanerozoic. *Geochim. Cosmochim. Acta* **70**, 5665–5675.

Scher H. D. and Martin E. E. (2006) Timing and climatic consequences of the opening of Drake Passage. *Science* **312**, 428–430.

Schopka H. H. and Derry L. A. (2012) Chemical weathering fluxes from volcanic islands and the importance of groundwater: the Hawaiian example. *Earth Planet. Sci. Lett.* **339–340**, 67–78.

Schopka H. H., Derry L. A. and Arcilla C. A. (2011) Chemical weathering, river geochemistry and atmospheric carbon fluxes from volcanic and ultramafic regions on Luzon Island, the Philippines. *Geochim. Cosmochim. Acta* **75**, 978–1002.

Stein R. (1990) Organic carbon content/sedimentation rate relationship and its paleoenvironmental significance for marine sediments. *Geo-Mar. Lett.* **10**, 37–44.

Timofeeff M. N., Lowenstein T. K., da Silva M. A. M. and Harris N. B. (2006) Secular variation in the major-ion chemistry of seawater: evidence from fluid inclusions in Cretaceous halites. *Geochim. Cosmochim. Acta* **70**, 1977–1994.

Tripati A. K., Roberts C. D. and Eagle R. A. (2009) Coupling of CO_2 and ice sheet stability over major climate transitions of the last 20 million years. *Science* **326**, 1394–1397.

Walker J. C. G., Hays P. B. and Kasting J. F. (1981) A negative feedback mechanism for the long-term stabilization of Earths surface temperature. *J. Geophys. Res.* **86**, 9776–9782.

Wallmann K. (2001) Controls on the Cretaceous and Cenozoic evolution of seawater composition, atmospheric CO_2 and climate. *Geochim. Cosmochim. Acta* **65**, 3005–3025.

West A. J., Galy A. and Bickle M. (2005) Tectonic and climatic controls on silicate weathering. *Earth Planet. Sci. Lett.* **235**, 211–228.

Willenbring J. K. and von Blanckenburg F. (2010) Long-term stability of global erosion rates and weathering during late-Cenozoic cooling. *Nature* **465**, 211–214.

Wu W. H., Yang J. D., Xu S. J., Li G. J., Yin H. W. and Tao X. C. (2009) Sr fluxes and isotopic compositions of the eleven rivers originating from the Qinghai-Tibet Plateau and their contributions to $^{87}Sr/^{86}Sr$ evolution of seawater. *Sci. China Ser. D.* **52**, 1059–1067.

Zachos J., Pagani M., Sloan L., Thomas E. and Billups K. (2001) Trends, rhythms, and aberrations in global climate 65 Ma to present. *Science* **292**, 686–693.

Zachos J. C., Dickens G. R. and Zeebe R. E. (2008) An early Cenozoic perspective on greenhouse warming and carbon-cycle dynamics. *Nature* **451**, 279–283.

Zimmermann H. (2000) Tertiary seawater chemistry – implications from fluid inclusions in primary marine halite. *Am. J. Sci.* **300**, 723–767.

Associate editor: Jerome Gaillardet